PROCESSING, MICROSTRUCTURE AND PROPERTIES OF 2–4 % Mn AND 0.3/0.7 % C SINTERED STEELS

EVA DUDROVÁ[1]*, MARGITA KABÁTOVÁ[1], RADOVAN BUREŠ[1], RÓBERT BIDULSKÝ[1], ANDREW S. WRONSKI[2]

[1] *Institute of Materials Research of the Slovak Academy of Sciences, Watsonova 47, 043 53 Košice, Slovak Republic*
[2] *Engineering Materials Group of the School of Engineering, University of Bradford, Richmond Road, West Yorkshire, BD7 1DP, United Kingdom*

Received 17 October 2005, accepted 14 November 2005

Powder mixes containing up to 4 % Mn with 0.3 or 0.7 % C, balance Fe, were compacted to green densities ranging from 7.0 to 7.1 $g \cdot cm^{-3}$ and sintered in atmosphere of N_2/H_2 in laboratory and industrial furnaces at temperatures of 1120–1200 °C and dew points ranging from −60 to −23 °C. Sinter-hardening was also investigated. All the alloy microstructures were heterogeneous, consisting of diffusive and non-diffusive transformation products and additionally ferrite and retained austenite. The best combination of mechanical properties for the industrially sintered furnace-cooled state, yield, tensile and bend strengths of 438, 580 and 1136 MPa, with tensile strain of 1.12 %, was achieved for Fe-2Mn-0.7C alloy. Sinter-hardening led to an improvement in mechanical properties: for Fe-4Mn-0.3C alloy the yield, tensile and bend strengths were 570, 664 and 1263 MPa, respectively, at acceptable impact energy of 14 J, with tensile strain of 0.52 %. Many of the results compare favourably with the requirements of MPIF 35 for medium strength structural parts.

K e y w o r d s: manganese sintered steels, microstructure, mechanical properties

1. Introduction

Manganese, because of its strengthening and hardenability properties, is a common alloying element in wrought steels, yet it has found scant application in powder metallurgy. Additionally, in terms of attainable mechanical properties, e.g. for materials for automotive precision transmission parts, Mn would be an efficient substitute for the currently employed expensive, carcinogenic and toxic nickel [1]

*corresponding author, e-mail: dudrova@imrnov.saske.sk

and the non-recyclable copper. Of the many previous, including recent, investigations [2–19], many have not identified, and therefore not solved, the problem of avoiding embrittling oxide networks. It has been shown that to achieve reproducible worthwhile mechanical properties in sintered Mn steels, it is necessary to avoid the formation of these networks, necessarily formed in flowing gases if the dew point favours oxidation of manganese during the sintering cycle [11, 12–17]. The dew point requirement, dictated by the Ellingham diagram, for pure hydrogen at 1120 ℃ and 1200 ℃ is −55 ℃ and −40 ℃, respectively, and for the mixed atmospheres, containing e.g. 25% hydrogen and balance nitrogen, it becomes theoretically −68 ℃ at 1120 ℃ and −53 ℃ at 1200 ℃, respectively.

As postulated by Mitchell et al. [17, 18, 20, 21], also Ortiz and Castro for Cr steels [22], the only effective way for a "good" sintering of Mn and Cr containing steels is an active "micro-climate" around and within the compacts. Cias et al. [21] have postulated that the relevant initial reactions are:

$$2\mathrm{Mn}_{(\mathrm{vapour})} + \mathrm{O_2} = 2\mathrm{MnO} \tag{1}$$

and

$$\mathrm{Mn}_{(\mathrm{vapour})} + \mathrm{H_2O}_{(\mathrm{vapour})} = \mathrm{MnO} + \mathrm{H}_{2(\mathrm{gas})}, \tag{2}$$

which results in the formation of H_2 in the microclimate. The oxide has been shown to be deposited on the inside of pores and not to be deleterious to mechanical properties, even if it is not subsequently reduced when the redox line is crossed. Carbon in the compacts (or in the getter) can produce H_2, CO_2 and CO, that can create carbothermic reactions and sintering in reducing conditions. These are controlled by the equilibrium ratio $p\mathrm{CO}/p\mathrm{CO_2}$ at a given temperature and oxygen content. When hydrogen and carbon are available, these reactions will also take place:

$$3\mathrm{Fe_2O_3} + \mathrm{H_2} = 2\mathrm{Fe_3O_4} + \mathrm{H_2O} \tag{3}$$

$$\mathrm{Fe_3O_4} + \mathrm{H_2} = 3\mathrm{FeO} + \mathrm{H_2O} \tag{4}$$

$$\mathrm{FeO} + \mathrm{H_2} = \mathrm{Fe} + \mathrm{H_2O} \tag{5}$$

$$\mathrm{MnO} + \mathrm{H_2} = \mathrm{Mn} + \mathrm{H_2O} \tag{6}$$

$$\mathrm{C} + \mathrm{O_2} = \mathrm{CO_2} \tag{7}$$

$$\mathrm{C} + \mathrm{CO_2} = 2\mathrm{CO} \tag{8}$$

Recently Stackpole developed sintered steels [7, 9, 10] with Mn contents up to 1.5 % and Mitchell et al [11, 12–18] carried out extensive experimental work on Fe-Mn-(Mo)-(Cr)-C system, backed by theoretical analyses of sintering in dry hydrogen-rich atmospheres and in dry nitrogen in semi-closed containers. The results include, for 2–4 % Mn steels containing up to 0.8 % C, $R_\mathrm{p}0.2$, R_m and bend

(apparent) strengths in the ranges of 295–580, 300–600 and 800–1260 MPa, respectively. Most recently Danninger et al. [19] reported for Fe-3Mn-0.3C steel (sintered at 1160 ℃ for 90 min in H_2 with density of 7.08 $g \cdot cm^{-3}$) yield and tensile strengths 509 and 599 MPa, tensile strain of 3.9 %, impact energy of 32.9 $J \cdot cm^{-2}$ and hardness of 196 HV 30.

This communication deals with experiments performed in laboratory tube and pusher furnaces (Fe-3Mn-0.7C steel) and in an industrial pusher furnace (Fe-(2–4)Mn-0.3/0.7C steels), that may assist in bringing nearer the exploitation of sintered Mn steels. The objectives were to investigate and correlate the effects of composition and processing conditions (including semi-closed containers for Fe-3Mn-0.7C steel and sinter-hardening for Fe-(2–4)Mn-0.3/0.7C steels) with microstructure, micro-composition and mechanical properties (tensile and bend strengths, plasticity, impact energy, hardness and fatigue) of the tested alloys.

2. Experimental materials and procedures

The base material employed was a commercial sponge plain iron powder, Höganäs SC 100.26. This powder was selected for its higher specific surface area in comparison with the atomized powder, thus having higher diffusivity during sintering and alloying. The other commercial raw materials were commercial medium carbon ferro-manganese Fe-77%Mn-1.4%C-1.3%O (from Elkem Ferromanganese Sauda, Norway) milled under N_2 protective atmosphere to yield 56 % of particles under 10 μm mean diameter (with O content of 0.1 %), CR 12 graphite powder (from GRAFITE, Netolice) with particle size distribution of 90 % up to 15.1 μm, 50 % up to 8.9 μm, 10 % up to 3.9 μm, and HW wax powder as lubricant. Powder mixtures were homogenized in a Turbula mixer. Four different specimen types, compacted to a green density of 7.0–7.1 $g \cdot cm^{-3}$, were prepared: "dog-bone" tensile (ISO 2740), rectangular 3-point bend, 55 × 10 × 6 mm^3 (ISO 3325), unnotched impact energy, 55 × 10 × 10 mm^3 (ISO 5754), and fatigue (ISO 3928).

Formulation and processing parameters of the alloy batches are presented in Table 1. Sintered specimens were tested in static tension and simple bending, both tests on a ZWICK 1387 machine at a crosshead speed of 1 mm/min, and in an impact energy tester ($W_{max} = 150$ J). Some tensile tests, with an extensometer for a gauge length of 30 mm, at an extension rate of 0.1 mm/min, were carried out to determine static Young's modulus, evaluated to be 110–130 GPa, values comparable to previously published data [13, 14]. The values should also be compared [23] to measurements by the resonance technique (Grindo Sonic MKS "Industrial") at University of Vienna for Fe-3Mn-0.7C specimens laboratory sintered at 1200 ℃, which were in the range 152–156 GPa. The failure tensile strain, the tensile failure strength (R_m), the transverse rupture strength (TRS), the maximum tensile strain

T a b l e 1. Formulation and processing parameters of the sintered steels tested

Batch No. and composition	Composition	Furnace type atmosphere type heat treatment	Sintering temperature time cooling rate	Dew point (effective) of sintering atmosphere
2 Fe-3Mn-0.7C	SC100.26 + ferro-manganese + graphite	Laboratory Carbolite ceramic tube $75H_2 + 25N_2$ (pure gases) flowing gas	1120 °C 60 min 10 °C/min	−60 °C (−56 °C)
3 Fe-3Mn-0.7C			1200 °C 60 min 10 °C/min	−60 °C (−56 °C)
Bg Fe-3Mn-0.6C		Pilot FHD pusher $75H_2 + 25N_2$ (dissoc. NH_3) only ceramic getter	1130 °C 90 min 10 °C/min	−23 °C (−19 °C)
7g Fe-3Mn-0.7C		Industrial, Cremer pusher $25H_2 + 75N_2$ (pure gases) semi-closed containers with getter: Al_2O_3 + 10 % FeMnC + 5 % graphite	1180 °C 40 min 10 °C/min	−55 °C (−42 °C)
6 Fe-3Mn-0.7C		Industrial, Cremer pusher $75H_2 + 25N_2$ (dissoc. NH_3) flowing gas	1180 °C 40 min 10 °C/min	−30 °C (−26 °C)
23 Fe-2Mn-0.3C		Industrial, Cremer pusher $25H_2 + 75N_2$ (pure gases) (a) flowing gas cooled at 10 °C/min *or* (b) flowing gas cooled at 55 °C/min tempered at 200 °C/60 min	1180 °C 40 min 10 °C/min (a) *or* 1180 °C 40 min 55 °C/min + 200 °C/60 min (b)	−55 °C (−42 °C)
27 Fe-2Mn-0.7C				
33 Fe-3Mn-0.3C				
37 Fe-3Mn-0.7C				
43 Fe-4Mn-0.3C				
47 Fe-4Mn-0.7C				

in bending and the elastic limit and the (true) fracture strength in bending (maximum tensile stress in bend) were also evaluated. Three-point bend tests were used to evaluate the conventionally reported $TRS = 3Fl/2wt^2$, where l is the test span, w is the width and t is a thickness of the specimens from the load at failure F, irrespective of, generally, preceding plastic deformation. The maximum tensile stress in bend ($\sigma_{(\mathrm{B})\max}$), however, is equal to TRS only for brittle specimens. In plastically deformed specimens the $\sigma_{(\mathrm{B})\max}$ was calculated assuming linear work-hardening rates [15, 23, 24].

Fatigue properties were determined on a Schenk tester in symmetric plane bending at $R = -1$, frequency = 1450 min^{-1}, with $N_\mathrm{C} = 10^7$.

Light and scanning electron microscopy (Tesla BS 340 with EDX LINK ISIS microanalyser) were employed for microstructural evaluations. The hardness (apparent) HV 10 was measured on the surfaces and in the cores of the sintered specimens.

3. Results

3.1 Fe-3Mn-0.7C sintered steel

The alloy chosen for the majority of the tests was Fe-3Mn-0.7C. Formulation and processing parameters of the tested batches 2, 3, Bg, 7g, 6 are presented in Table 1. Green compacts with densities between 7.0 and 7.1 $\mathrm{g\cdot cm^{-3}}$ were laboratory sintered at temperatures of 1120, 1130 and 1200 ℃ in H_2-rich atmospheres with dew points of −60 ℃ or −23 ℃, and industrially at 1180 ℃ in H_2-rich atmospheres with dew points of −55 ℃ (batch 7g in a container with a getter containing ferromanganese and graphite) or with dew point of −30 ℃ in a flowing atmosphere. The cooling rates from sintering temperature were 10 ℃/min.

Table 2 presents the green and sintered densities, dimensional changes, Mn and C contents for batches 2, 3, Bg, 7g, 6, respectively. The data show that sintered specimens exhibited some swelling in the range from 0.23 to 0.46 % during the sintering cycle. The lowest dimensional change, 0.23 %, was exhibited by laboratory

Table 2. Green and sintered densities, dimensional changes, Mn and C contents in 3Mn0.7C batch of specimens

Batch	Density [$\mathrm{g\cdot cm^{-3}}$]		Dimensional changes [%]	Mn [wt.%]	C [wt.%]
	Green	Sintered			
2	7.09	7.03	+ 0.23	2.7	0.62
3	7.09	7.04	+ 0.23	2.7	0.63
7g	6.96	6.84	+ 0.46	3.0	0.65
6	7.09	6.94	+ 0.35	2.9	0.60
Bg	6.93	6.78	+ 0.42	2.79	0.48

Table 3. Area fractions of structural constituents of the 3Mn0.7C batch specimens sintered at 1120–1200 °C

1120 °C/60 min; Carbolite, dew point −60 °C, cooled at 10 °C/min (batch 2)		1200 °C/60 min; Carbolite, dew point −60 °C, cooled at 10 °C/min (batch 3)		1180 °C/40 min; Cremer, dew point −30 °C cooled at 10 °C/min (batch 6)	
Type	Area fraction [%]	Type	Area fraction [%]	Type	Area fraction [%]
ferrite	∼ 3.5	ferrite	∼ 1.5	ferrite	∼ 1.5
pearlite	∼ 77.5	pearlite-bainite	∼ 48.5	pearlite-bainite	∼ 43.5
austenite + martensite	∼ 9	austenite + martensite	∼ 40	austenite + martensite	∼ 45

Porosity: ∼ 10 % of area fraction

sintered specimens in an atmosphere with the dew point of −60 °C (batches 2 and 3); the highest swelling was detected for specimens sintered in a semi-closed container (batch 7g). The Mn and C contents in sintered specimens were measured by standard chemical techniques. The relative Mn loss during the sintering was up to 10 %; no Mn loss was detected for specimens sintered in a semi-closed container (batch 7g). Relative C loss was 7–20 %; the highest value was detected for specimens sintered in "poor" atmosphere (batch Bg). Microscopic observations showed the preferential Mn and C losses near the specimen surfaces.

Microstructures of all batches were complex and heterogeneous. The area fractions of constituents in alloys sintered at 1120, 1200 and 1180 °C are recorded in Table 3. Specimens sintered at 1120 °C, Fig. 1a, exhibited a predominantly pearlitic microstructure with small area fractions of ferrite (3.5 %) and austenite-martensite (9 %). The microstructure of specimens sintered at 1200 and 1180 °C, Fig. 1b, consisted of pearlite, bainite, martensite and austenite; the area fraction of retained austenite and martensite increased to ∼ 40 % as a substantial reduction of ferritic areas occurred. In the case of specimens sintered in a semi-closed container, the tendency to carbide phase formation at grain boundaries was detected, which can be explained by the higher carbon content and probably also by lower cooling rate of specimens from the sintering temperature.

EDX maps of specimen microstructures showed that the manganese distribution coincides with "dissolution" of ferromanganese particles, depending on the sintering temperature (Figs. 2a,b). The oxygen distribution is related to the "residuals" of ferromanganese particles (Fig. 2c). At the sintering temperature of 1200 °C and the dew point of −60 °C, oxides and silicates based on Si, Al, and Ti were present, which elements were introduced by the medium-carbon ferromanganese powder. The maps of the oxygen distribution in the case of industrial sintering (1180 °C, dew point −30 °C) showed that some oxide networks were formed prefer-

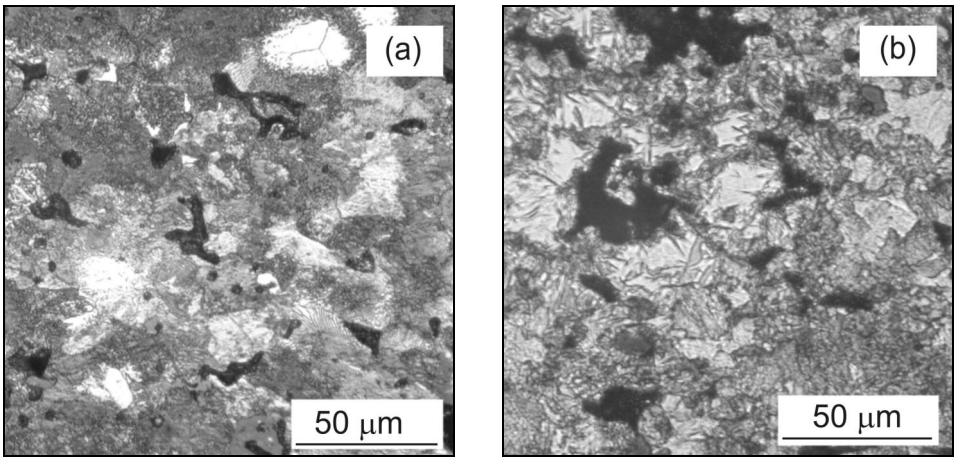

Fig. 1. Microstructures of the Fe-3Mn-0.7C alloy: (a) sintered at 1120 °C, dew point −60 °C, batch 2; (b) sintered at 1200 °C, dew point −60 °C, batch 3.

Table 4. Mechanical properties of the Fe-3Mn-0.7C batch of specimens

Batch	$R_p0.2$ [MPa]	Elastic limit in bend [MPa]	Tensile strain (total) [%]	Max. tens. strain in bend [%]	*TRS* [MPa]	Tensile failure strength [MPa]	Max. tens. stress in bend [MPa]	Hardness HV 10		Impact energy [J]
								Surface	Core	
2	327	374	1.69	2.93	860	478	572	168	153	12.5
3	490	550	1.02	0.82	1256	642	702	180	207	11
Bg	brittle	739	brittle	brittle	739	470	739	156	199	6
7g	450	498	1.30	2.8	1150	522	943	183	197	12
6	433	478	0.38	1.16	948	522	510	182	238	7

entially in the surfaces of the microvolumes of the original powder particles. Figure 2 illustrates these networks, which are avoided by "correct" processing.

Table 4 presents strength properties of the Fe-3Mn-0.7C materials (but batch Bg with 0.6 % C). The yield, tensile and bend strengths for this group of specimens were 327–490 MPa, 470–642 MPa and 739–1256 MPa, respectively; hardness ranged from 153 to 238 HV 10 and impact energy from 6 to 16 J. The positive effects of the higher sintering temperature and dry atmosphere (batch 3 specimens) are reflected by the highest achieved values of the yield, tensile and bend strengths, 490, 642 and 1256 MPa, respectively, at hardness of 207 HV 10 and an acceptable impact

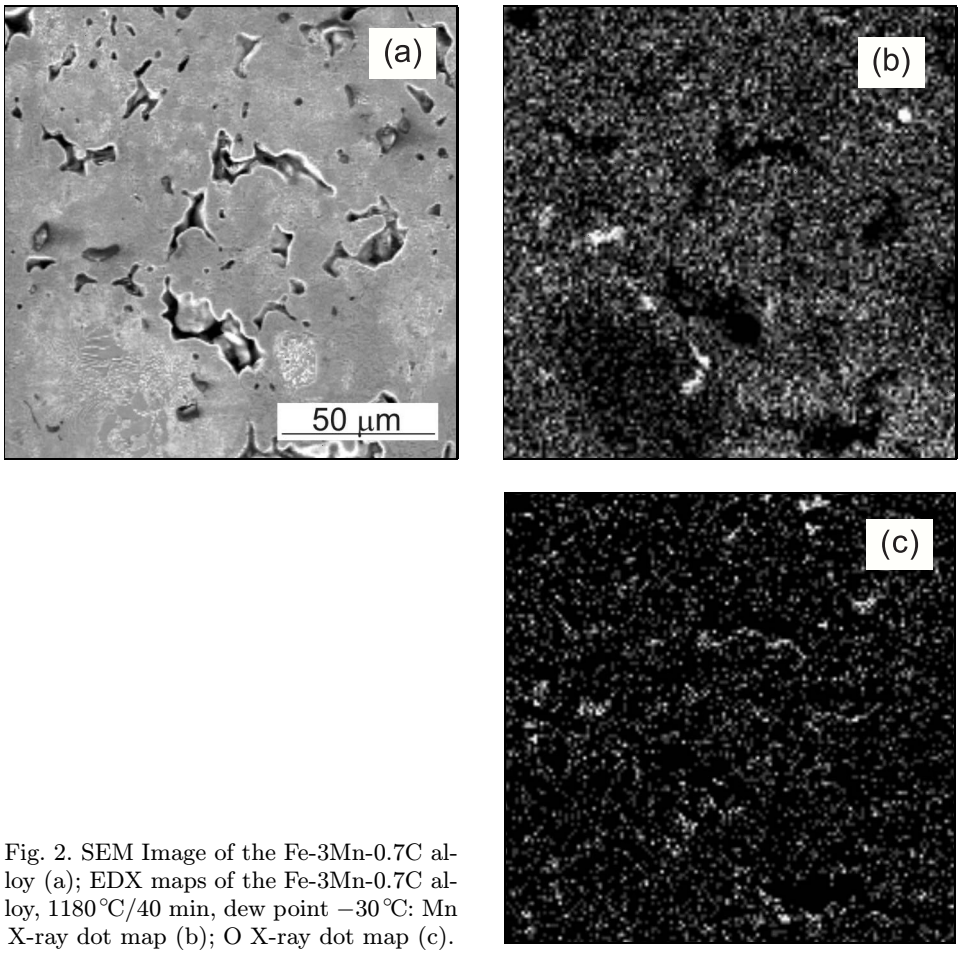

Fig. 2. SEM Image of the Fe-3Mn-0.7C alloy (a); EDX maps of the Fe-3Mn-0.7C alloy, 1180 °C/40 min, dew point −30 °C: Mn X-ray dot map (b); O X-ray dot map (c).

energy of 11 J. Using lower sintering temperature (batch 2 specimens) leads to lower yield, tensile and bend strengths, 327, 478 and 860 MPa, respectively, but to highest tensile strain, 1.69 %, and respectable impact energy of 12.5 J. The fracture surfaces of the more ductile specimens consisted mainly of dimple ductile facets with localized plastic deformation along with some transgranular cleavage facets, e.g. Fig. 3a for a batch 2 specimen. Some intergranular facets were detected on fracture surfaces of batch 6 specimens sintered in an industrial furnace in a flowing atmosphere having a dew point of −30 °C, e.g. Fig. 3b.

It should be added that the mechanical properties of the 7g specimens, industrially sintered in a "dry" atmosphere with the dew point of −55 °C, are comparable with those of batch 3 specimens laboratory sintered at 1200 °C in a dry flowing atmosphere.

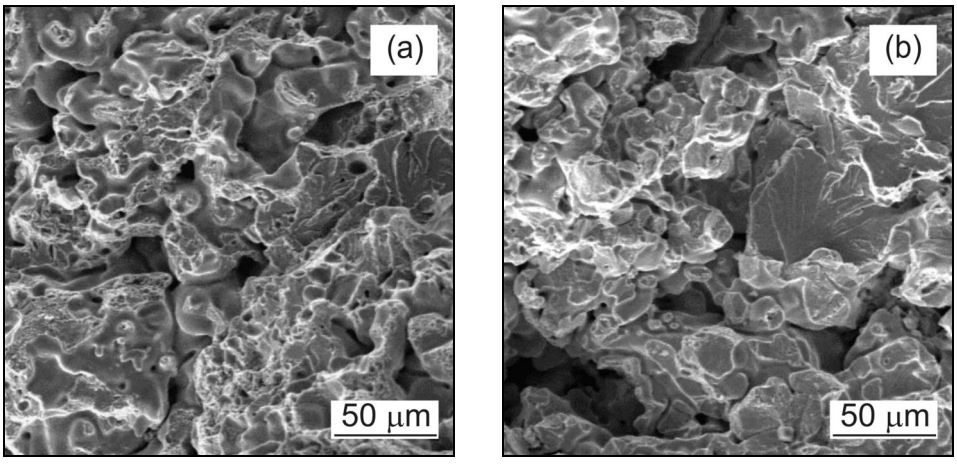

Fig. 3. Micrographs of fracture surfaces of: (a) batch 2 (1120 °C/60 min; dew point −60 °C); (b) batch 6 (1180 °C/40 min; dew point −30 °C).

The batch of Bg specimens, sintered in a "poor and wet" atmosphere having the dew point of −23 °C in an open container with only ceramic getter at 1130 °C for 90 min, exhibited brittle behaviour with tensile and bend strengths of only 470 and 739 MPa, respectively, and a low impact energy of 6 J. The negative effect of "wet" inadequately gettered atmosphere resulted in oxide networks formation along the grain boundaries. Their presence is responsible for the lower plasticity of the samples sintered in an atmosphere with a low oxidic cleanliness.

The value of 0.2 % offset yield strength determined in tension was generally somewhat lower than the apparent proportional limit determined in bending for each set of specimens.

The reproducibility of tensile and *TRS* data (determined for batches 2, 3, 6), was characterized by Weibull modulus, m, of 15–28.

3.2 2–4 % Mn and 0.3/0.7 % C sintered steels

Formulation and processing parameters of the Fe-2–4Mn-0.3/0.7C industrially sintered steels are presented in Table 1. Industrial sintering in a Cremer pusher furnace (Metalsint, a.s., Dolný Kubín) was carried out at the temperature of 1180 °C for 40 min, in an atmosphere of 25 % H_2 + 75 % N_2 (obtained from a cryogenic liquid). The inlet dew point was −55 °C. Specimens (a) were furnace cooled at ∼ 10 °C/min. To simulate "sinter-hardening", specimens (b) were reheated to 900 °C and air-cooled at ∼ 55 °C/min (in the range 900 to 400 °C) and then tempered at 200 °C for 60 min.

Table 5. Green and sintered densities, dimensional changes, Mn and C contents in 2–4 % Mn and 0.3/0.7 % C sintered and slow-cooled alloy specimens

Alloy	Density [g·cm^{-3}]		Dimensional change	Mn	C
	Green	Sintered	[%]	[%]	[%]
23a	7.06	7.08	0.00	1.84	0.27
27a	7.06	7.03	+ 0.18	1.90	0.64
33a	7.09	7.04	+ 0.16	2.78	0.28
37a	7.03	6.96	+ 0.31	3.01	0.68
43a	7.08	6.98	+ 0.41	4.04	0.30
47a	7.04	6.90	+ 0.57	4.03	0.68

Table 6. Area fractions of microstructural constituents in slow-cooled (a) and sinter-hardened (b) batch of specimens

Constituent	Area fraction of microstructural constituents [%] in the alloy					
	23a/23b	33a/33b	43a/43b	27a/27b	37a/37b	47a/47b
ferrite	∼ 39/∼ 35	∼ 26/∼ 23	∼ 11/∼ 9	∼ 2/∼ 2	∼ 1/∼ 1	∼ 1/∼ 1
pearlite+bainite	∼ 46/∼ 49	∼ 53/∼ 60	∼ 70/∼ 72	∼ 55/∼ 56	∼ 46/∼ 48	∼ 46/∼ 35
martensite+austenite	∼ 5/∼ 6	∼ 7/∼ 7	∼ 9/∼ 9	∼ 33/∼ 32	∼ 43/∼ 40	∼ 43/∼ 54

The green and sintered densities, dimensional changes, Mn and C contents in the Fe-2–4Mn-0.3/0.7C alloy specimens are given in Table 5. Specimens of sintered and slow-cooled Fe-2Mn-0.3C alloys (batch 23a) had no dimensional change, whereas the Fe-(3 and 4)Mn-(0.3 and 0.7)C steels exhibited some swelling, 0.16–0.57 %, which increased with an increase in both Mn and C contents. Slightly higher swelling was detected in the sinter-hardened specimens. Mn and C losses were up to 10 %.

All slow-cooled and sinter-hardened microstructures were complex and inhomogeneous. The area fractions of the microstructural constituents of both slow-cooled and sinter-hardened alloys are given in Table 6. The microstructures of slow-cooled 2–4 % Mn alloys with 0.3 % C consisted of ferritic areas with pearlitic rims, fine and coarse bainite and some martensite and retained austenite, e.g. Fig. 4a for the Fe-4Mn-0.3C alloy. An increase in the Mn content from 2 to 4 % resulted in a decrease of ferrite area fraction from ∼ 39 to ∼ 11 %, whereas the fraction of martensite + austenite areas increased from ∼ 5 to ∼ 9 %. Microstructures of the slow-cooled Fe-(2–4)Mn-0.7C specimens were a mixture of fine and coarse pearlite, bainitic structures martensite and retained austenite. Only small ferrite areas were identified in the interiors of the largest iron particles, e.g. Fig. 4c, for batch 27a of the Fe-2Mn-0.7C alloy.

The sinter-hardened microstructure of 2–4 % Mn alloys with 0.3 % C, similarly

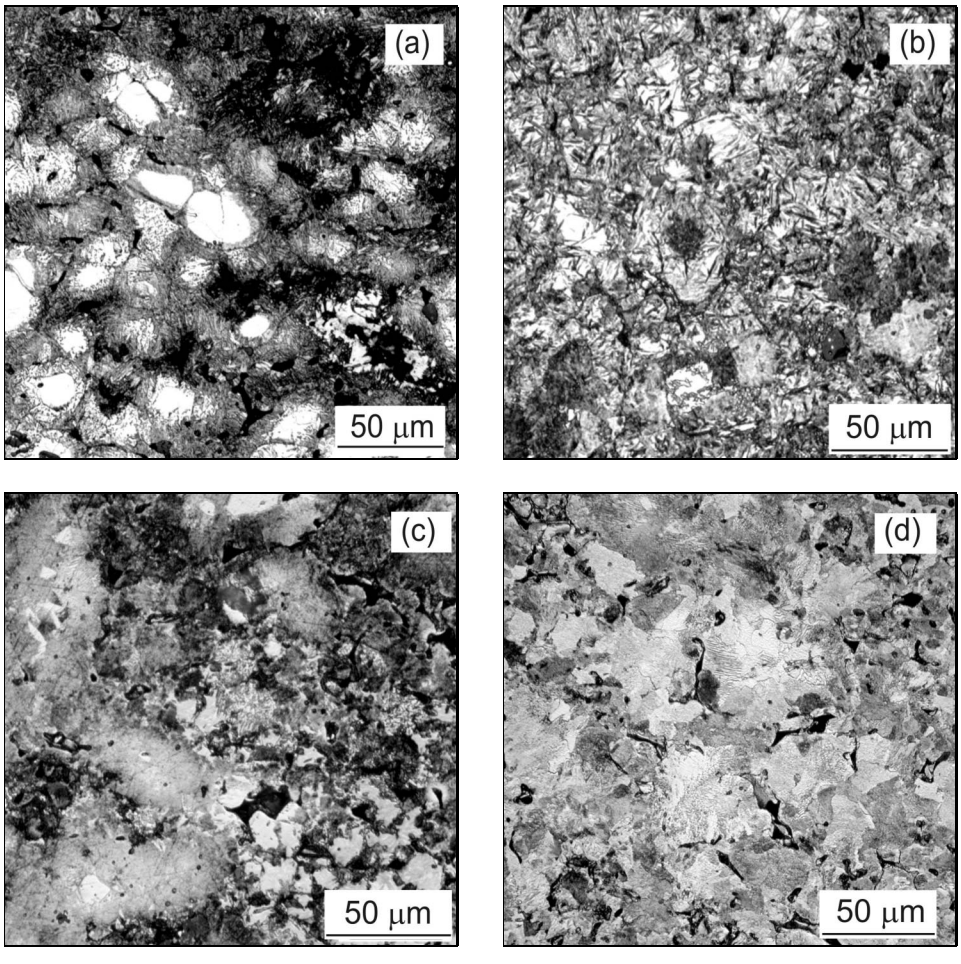

Fig. 4. Microstructures of the alloys: (a) Fe-4Mn-0.3C slow cooled, batch 43a; (b) Fe-4Mn-0.7C sinter-hardened, batch 47b; (c) Fe-2Mn-0.7C slow cooled, batch 27a; (d) Fe-2Mn-0.7C sinter-hardened, batch 27b.

to the slow-cooled state, consisted of ferritic areas with pearlitic rims. As a result of the higher cooling rate, the pearlite was finer in comparison with slow-cooled microstructures and, in addition to upper bainite, lower bainite was present. The microscopically evaluated area fraction of the pearlitic + bainitic microstructures exhibited only little change. An increase of Mn content from 2 to 4 % resulted in a decrease of the ferrite area fraction from $\sim$ 35 to $\sim$ 2 %, whereas the area fraction of martensite + retained austenite increased from $\sim$ 6 to $\sim$ 9 %. Increasing Mn content

T a b l e 7. Mechanical properties of the Fe-(2,3,4)Mn-(0.3/0.7)C batches of specimens

Batch	$R_p0.2$ [MPa]	Elastic limit in bend [MPa]	Tensile strain (total) [%]	Max. tens. strain in bend [%]	*TRS* [MPa]	Tensile failure strength [MPa]	Max. tens. stress in bend [MPa]	Hardness HV 10		Impact energy [J]
								Surface	Core	
23a	388	413	1.30	2.90	958	473	761	170	172	20
27a	438	512	1.12	2.31	1136	580	925	186	181	16
33a	449	503	0.48	1.30	994	524	812	190	195	9
37a	435	487	0.23	2.30	1123	569	917	189	208	9
43a	brittle	966	brittle	brittle	966	501	brittle	212	210	8
47a	450	502	0.30	0.96	867	481	690	229	253	7
23b	412	459	1.50	3.40	1091	498	870	168	173	20
27b	489	542	0.70	2.93	1148	572	900	177	203	15
33b	430	497	1.12	2.70	1108	557	965	202	194	17
37b	557	623	0.37	1.90	1151	602	999	222	234	13
43b	570	547	0.52	1.80	1263	664	1027	230	287	14
47b	471	525	0.39	1.62	1066	540	873	236	273	15

to 4 % at 0.7 % C resulted in predominantly bainitic-martensitic microstructures with a relatively high portion of lower bainite, e.g. Fig. 4b for batch 47b specimen.

EDX maps of oxygen distribution showed that oxide networks were not generally detected after sintering at 1180 ℃ with the dew point of −55 ℃. Some oxide phase was found only in the case of the Fe-4Mn-0.3C slow-cooled alloy.

The mechanical properties of specimens which were slow-cooled and sinter-hardened are recorded in Table 7. Of the slow-cooled alloys, only Fe-4Mn-0.3C exhibited brittle behaviour; all the sinter-hardened specimens were ductile.

3.2.1 Effect of Mn content: 2, 3 and 4 %

Comparing slow-cooled specimens at 0.3 % C level, increasing Mn from 2 to 4 % (batches 23a, 33a, 43a) resulted in a slight strength increase only for 3 % Mn and in a decrease for 4 % Mn alloy, which exhibited completely brittle behaviour, associated with predominantly intergranular type of failure, due to some oxide phase at grain boundaries. Inclusions with high manganese and oxygen (identified by EDX analysis) contents were detected on the intergranular failure facets, e.g. Fig. 5a. In contrast, fracture surfaces of the Fe-(2–3)Mn-0.3C slow-cooled specimens (similarly of the sinter-hardened specimens), in accordance with some plasticity being detected, consisted of ductile facets with localized plastic flow, Fig. 5b.

At 0.7 % C level, the highest strength, ductility and impact energy were

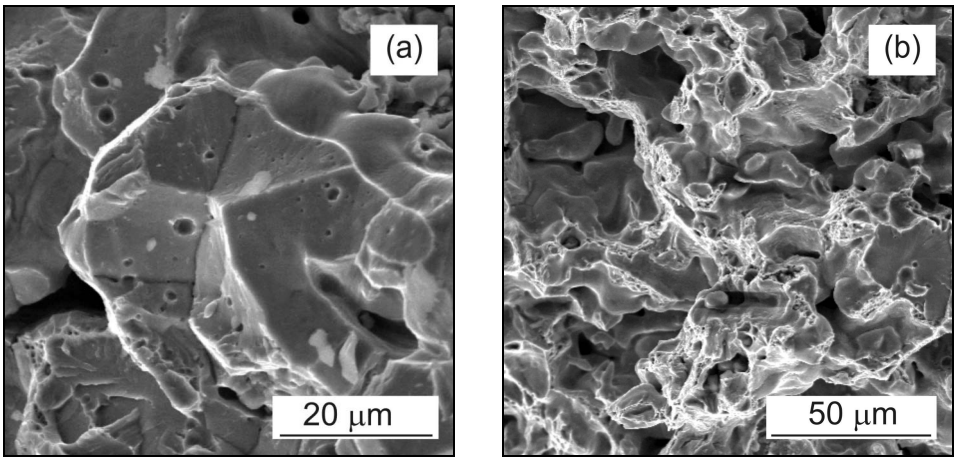

Fig. 5. Micrographs of fracture surface of the alloys: (a) Fe-4Mn-0.3C, slow cooled, batch 43a; (b) Fe-2Mn-0.3C, slow cooled, batch 23a.

Table 8. Weibull moduli, m, for tensile and bend strengths values of the tested slow-cooled and sinter-hardened 2–4 % Mn alloys

Batch	23a	33a	43a	27a	37a	47a	23b	33b	43b	27b	37b	47b
R_m	40	29	20	22	20	14	10	27	28	25	33	21
TRS	41	28	17	25	13	14	23	26	23	21	33	19

achieved for the 2 % Mn alloy. Comparing sinter-hardened specimens at 0.3 % C level, increasing Mn from 2 to 4 % (batches 23b, 33b, 43b) resulted in an increase of strength, by about 20 %, whereas ductility and impact energy decreased. At 0.7 % C level the strength slightly increased for 3 % Mn, and slightly decreased for 4 % Mn. In the case of Fe-(2–3)Mn-0.7C, due to the higher area fraction of high strength structures, some cleavage fracture was detected. The Fe-4Mn-(0.3; 0.7)C sinter-hardened alloys fractured by a mixture of transgranular cleavage, intergranular and some small ductile failure modes. Ductility decreased with higher Mn contents and impact energy did not significantly change.

The reproducibility of tensile and *TRS* data was high for sintered materials, characterized by Weibull modulus, m, of 10–41, for slow-cooled and sinter-hardened specimens, Table 8.

3.2.2 *Effect of C content: 0.3 and 0.7 %*

Comparing slow-cooled specimens at 2 % Mn level, increasing C from 0.3 to 0.7 % (batches 23a and 27a) resulted in strength increases of about 30 % and slight

decreases of ductility and impact energy. At 3 % Mn level, batches 33a and 37a, however, there was no such pattern; the effect of C was negligible. At 4 % Mn (batches 43a and 47a) the C effect was reversed, whereas the low C specimens were brittle, the 4%Mn-0.7%C steel recorded some plasticity at the same strength level. Comparing sinter-hardened specimens at 2 % Mn level, increasing C from 0.3 to 0.7 % C (batches 23b and 27b) increases the strength by about 15 %, accompanied by decreases of ductility (by 50 %) and impact energy. At 3 % Mn level (batches 33b and 37b) the strength slightly increased, while the ductility and impact energy decreased. At 4 % Mn level (batches 43b and 47b) the strength decreased by about 15 %, ductility slightly decreased, while the impact energy did not change. Generally the results compare favourably with previous data on Fe-3Mn-0.5/0.6 steels [25].

3.3 Fatigue strength

Fatigue strength was evaluated by Wöhler curves for the plane bending fatigue tests on unnotched specimens of selected slow-cooled and sinter-hardened alloys. The fatigue strengths at $N_C = 10^7$ were 140, 160 and 175 MPa for the Fe-2Mn--0.3C, Fe-3Mn-0.3C and Fe-3Mn-0.7C slow-cooled alloys, respectively, and 230 MPa for the Fe-3Mn-0.7C sinter-hardened alloy. The strength ratios were 0.38–0.41 for σ_c/R_m, and 0.15–0.20 for σ_c/TRS. These fatigue strengths are to be compared to values in the range 125 to 150 MPa for Fe-(2/3)Mn-(0.3/0.7)C steels laboratory sintered in "poor" atmospheres [26] and values of 164–240 MPa for sintered steels based on Distaloy AE + 0.6 % C powder [27, 28].

4. Discussion

It appears that there is no simple relation between mechanical properties and Mn and C contents of the PM steel compositions studied; details of the complex microstructures and failure micromechanisms need to be considered, especially in the context of hardenability and embrittlement mechanisms [29].

The deleterious effect of high manganese content at a low carbon level was most pronounced in the case of the Fe-4Mn-0.3C slow-cooled alloy, which exhibited completely brittle behaviour associated with predominantly intergranular type of failure due to the oxide phase at grain boundaries. It should be borne in mind that manganese diffusion in the iron matrix is more effective along grain boundaries than by volume diffusion and that manganese oxides that form on the surfaces of pores are benign [14]. One interpretation of the brittle behaviour of Fe-4Mn--0.3C slow-cooled specimens associates it with the transport of manganese vapour, formed at $\sim$ 700 °C (e.g. 20), through the interconnected pores. It is possible that the carbothermic reactions [20], due to the high Mn and low C contents, did not completely eliminate MnO during the heating stage of the sintering cycle. More

probably, as the ratio $p\mathrm{CO}/p\mathrm{CO_2}$ is shifted to oxidizing conditions during the slow cooling, manganese could be re-oxidized to form oxides on grain and/or prior particle boundaries.

Additionally it should be stressed that the ferro-manganese contained slag, which was not completely eliminated by the milling and sieving processes. Accordingly some of the oxygen present is associated with spinels $\mathrm{FeO \cdot SiO_2}$, $\mathrm{FeAl_2O_4}$, $\mathrm{Fe_2Al_4Si_5O_{18}}$, again preferentially present at the boundaries. The presence of such spinels could be expected also in an iron sponge powder and Fig. 6 shows "marked" grain boundaries situated close to a prior ferro-manganese particle.

Generally plasticity of Mn sintered steels processed from powder mixtures (especially if sponge iron powders are used) is lower than that for Ni-Cu-Mo steels. In some instances, even if "correct" processing is employed, this may be accounted for by re-oxidation during cooling, as discussed above. Increasing the manganese content increases the number of sites for embrittling the grain boundaries with the negative effect on plastic properties becoming more pronounced. Accordingly use of atomized iron powders could be more advantageous than of sponge, the manganese (more effective ferrite strengthener than Ni) content need not be higher than 3 % and the element should be added as atomic (electrolytic) Mn or gas atomized Fe-Mn-C master alloy [30]. At this addition the extra costs, compared to using ferro-manganese, are not considered to be significant.

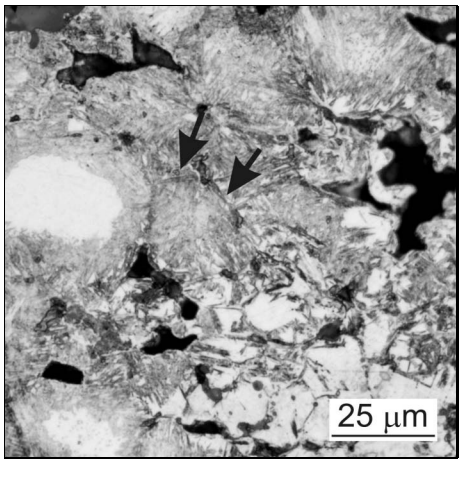

Fig. 6. "Marked" grain boundaries near upon the manganese source in the Fe-4Mn--0.3C slow cooled alloy, batch 43a.

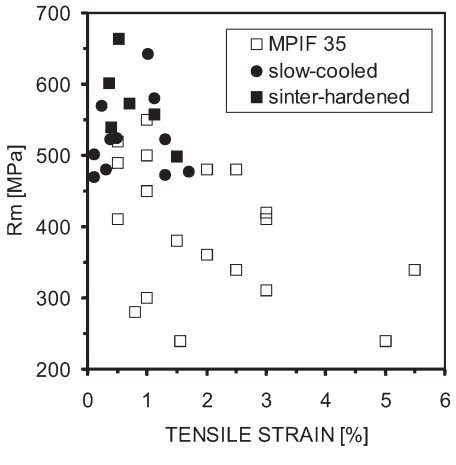

Fig. 7. Comparison between tensile strengths and tensile strains for steels specified in MPIF Standard 35 and the investigated Mn alloyed steel specimens.

Finally we need to consider the properties of these Mn steels in comparison with the Cu, Ni and Mo containing steels for medium-strength structural materials, according to the MPIF Standard 35. In Fig. 7 strength is plotted versus strain for those alloys and the novel Mn steel. It is seen that the ductilities of Standard 35 materials appear higher than of the Mn steel now studied, but the strengths are comparable or higher. Regarding mechanical properties, Mn is superior to Cu. Accordingly, considering Ni additions only, i.e. absence of Cu, for comparable densities, our PM Mn steel is stronger, though Ni steels are more ductile.

Improvements in processing technology and adjustments of composition, including addition of Cr, which PM alloying element can now also be successfully PM processed, should enable successful exploitation of Mn steels.

5. Conclusions

All microstructures of the Fe-(2,3,4)%Mn-(0.3/0.7)%C sintered alloys were heterogeneous, consisting of the diffusive and non-diffusive transformation products and additionally ferrite and retained austenite. The sinter-hardened microstructures, resulting from the higher cooling rate, consisted of higher area fractions of lower bainite, martensite and some austenite.

The mechanical properties of the now studied Fe-3Mn-0.7C steel can be summarized thus:

– The yield and tensile strengths were in the range from 327 to 490 MPa and 470 to 642 MPa, impact energy from 6 to 12.5 J, bend strength (apparent) from 739 to 1256 MPa, which transforms to (true) bend fracture strength ranging from 510 to 943 MPa. The hardness (apparent) ranged from 153 to 238 HV 10. The highest strength properties were recorded for laboratory sintering in dry atmosphere at 1200 ℃ ($R_p0{,}2 = 490$ MPa, $R_m = 642$ MPa and $TRS = 1256$ MPa, which transforms to (true) fracture strength of 702 MPa).

– Plasticity was recorded for all groups of specimens sintered in a dry atmosphere, or in semi-closed containers with an effective (containing Mn and C) getter. Tensile and maximum bend strains were 1.69 and 2.93 % for specimens sintered at 1120 ℃. Specimens sintered at 1200 ℃ exhibited higher strength, but the plasticity was lower, 1.02 %.

– Sintering in a "wet" atmosphere, with a dew point of −23 ℃, resulted in a brittle behaviour.

The mechanical properties of the now tested Fe-(2–4)Mn-(0.3/0.7)C steels can be summarized as follows:

– The highest yield, tensile and bend strengths in slow-cooled alloy compositions of 438, 580 and 1136 MPa, respectively, at impact energy 16 J, and tensile and bend strains of 1.12 and 2.31 % were recorded for alloying with 2 % Mn and 0.7 % C.

– Excluding the brittle failures of Fe-4Mn-0.3C alloys, specimens fractured by ductile and transgranular cleavage modes. The hardness of the alloys tested in slow-cooled state was in the range from 172 to 253 HV 10.

– Sinter-hardening leads to some improvement in the mechanical properties; the highest yield, tensile and bend strengths of 570, 664 and 1263 MPa, respectively, at an acceptable impact energy of 14 J, and tensile and bend strains of 0.52 % and 1.8 % were achieved for the Mo-free Fe-4Mn-0.3C alloy.

– The fatigue strengths for the Fe-3Mn-0.3 and 0.7C slow-cooled alloys were 160 and 175 MPa, respectively, and 230 MPa for the Fe-3Mn-0.7C sinter-hardened alloy. These values are in the range of fatigue strengths for sintered steels based on Distaloy AE powder with 0.6 % C (164–240 MPa) [27, 28].

The reproducibility of tensile and TRS results was, for PM materials, high, characterized by Weibull moduli, m, of 10–41.

Many of these results compare favourably with the requirements of MPIF Standard 35. Mn is a more effective strengthening agent than either Ni or Cu, or their combination, though generally at reduced plasticity.

Acknowledgements

Paper based on the presentation at the Conference RoPM 2005, Sinaia, Romania, 7–9 July 2005. The authors acknowledge provision of a Cremer industrial pusher sintering furnace for this investigation by Ing. A. Čajka of Metalsint, a.s., Dolný Kubín. The authors also thank Prof. D. Rodziňák for conducting the fatigue tests. The project, part of the ongoing collaboration between IMR SAS Košice and the University of Bradford, was financially supported by a NATO Science for Peace Grant No 972395, and by the Slovak Grant Agency for Science, Project VEGA 2/3207/23.

REFERENCES

[1] EU Carcinogen Directives 90/394/EEC and 91/322/EEC.
[2] ZAPF, G.—HOFFMANN, G.—DALAL, K.: Arch. Eisenhüttenwes., *46*, 1975, p. 287.
[3] ŠALAK, A.: Powder Metall. Int., *2*, 1980, p. 72.
[4] KLEIN, A. N.—OBERACKER, R.—THÜMMLER, F.: Powder Metall. Int., *7*, 1985, p. 13.
[5] CAMINHA, I. M. V.—RIZZO ASSUNCAO, F. C.: In: Int. Conference on Powder Metallurgy – 1990. Vol. 3. London, The Institute of Metals 1990, p. 94.
[6] OBERACKER, R.: Powder Metall. Int., *22*, 1990, p. 54.
[7] SCHAFFLER, D. J.—LAWLEY, A.—CAUSTON, R. J.: In: PM'92 World Congress on Powder Metallurgy. Eds.: Capus, J. M., German, R. M. Vol. 15. San Francisco, MPIF Princeton NJ 1992, p. 93.
[8] DANNINGER, H.: In: PM'94 Powder Metallurgy World Congress. Vol. 2. Paris, Sociéte Francaise de Métallurgie et Matériaux, EPMA 1994, p. 879.
[9] SHIVANATH, R.—JONES, P. K.—LAWKOCK, R.: In: Advances in Powder Metallurgy & Particulate Materials – 1996. Eds.: Cadle, T., Narasimhan, S. Vol. 4–13. Washington D.C., MPIF Princeton NJ 1996, p. 427.

[10] JONES, P. K.—GODERODER, K. B.—LAWCOCK, R.—SHIVANATH, R.: In: Advances in Powder Metallurgy & Particulate Materials – 1996. Eds.: Cadle, T., Narasimhan, S. Vol. 4–13. Washington D.C., MPIF Princeton NJ 1996, p. 439.
[11] CIAS, A.—MITCHELL, S. C.—WRONSKI, A. S.: In: PM'98 Powder Metallurgy World Congress on Powder Metallurgy. Vol. 3. Granada, Shrewsbury, EPMA 1998, p. 179.
[12] CIAS, A.—MITCHELL, S. C.—WRONSKI, A. S.: Powder Metall., *42*, 1999, p. 227.
[13] WRONSKI, A. S.—CIAS, A.—BARCZY, P.—STOYTCHEV, M.: Final Report on EU Copernicus Contract CIPA CT-94-0108, European Commission 1998.
[14] MITCHELL, S. C.: The Development of Powder Metallurgy Manganese Containing Low-Alloy Steels. [Ph.D. Thesis]. University of Bradford 2000.
[15] MITCHELL, S. C.—WRONSKI, A. S.—CIAS, A.: Inżynieria Materialowa, *22*, 2001, p. 633.
[16] CIAS, A.—STOYTCHEV, M. —MITCHELL, S. C. —WRONSKI, A. S.: In: 2001 Advances in Powder Metallurgy & Particulate Materials. Eds.: Eisen, W. B., Shiz Kassam. New Orleans, MPIF Princeton NJ 2001, Part 10, p. 131.
[17] CIAS, A.—MITCHELL, S. C.—PILCH, K.—CIAS, H.—SULOWSKI, M. —WRONSKI, A. S.: Powder Metall., *46*, 2003, p. 165.
[18] MITCHELL, S. C.—STOYTCHEV, M.—SELECKÁ, M.: Final report on NATO Project Science for Peace, PN 972395, 2003.
[19] DANNINGER, H.—PÖTTSCHACHER, R.—BRADAC, S.—ŠALAK, A.—SEYRKAMMER, J.: Powder Metall., *48*, 2005, p. 23.
[20] MITCHELL, S. C.—CIAS, A.: Powder Metallurgy Progress, *4*, 2004, p. 132.
[21] CIAS, A.—MITCHELL, S. C.—WRONSKI, A. S.: In: EURO PM2004, Powder Metallurg World Congress & Exhibition. Eds.: Danninger, H., Ratzi, R. Vol. 2. Vienna, EPMA 2004, p. 5.
[22] ORTIZ, P.—CASTRO, F.: Powder Metall., *47*, 2004, p. 291.
[23] WRONSKI, A. S.—OLIVEIRA, M. M.: Inżynieria Materialowa, *19*, 1998, p. 1123.
[24] WRONSKI, A. S.—CIAS, A.: In: EURO PM2004, Powder Metallurg World Congress & Exhibition. Eds.: Danninger, H., Ratzi, R. Vol. 3. Vienna, EPMA 2004, p. 1.
[25] PIECZONKA, T.—MITCHELL, S. C.—SULOWSKI, M.—WRONSKI, A. S.—CIAS, A.: Inżynieria Materialowa, *19*, 1998, p. 1171.
[26] RODZIŇÁK, D.—DUDROVÁ, E.—KABÁTOVÁ, M.: Kovove Mater., *41*, 2003, p. 416.
[27] ENGSTRÖM, U.—LINDBERG, G.—TENGZELIUS, J.: Powder Metall., *3*5, 1992, p. 67.
[28] LINDNER, K. H.—SONSINO, C. M.: Mat.-Wiss. und Werkstofftechnik, *25*, 1994, p. 227.
[29] CIAS, A.—MITCHELL, S. C.: In: Deformation and Fracture in Structural PM Materials, DFPM 2005. Eds.: Parilák, Ľ., Danninger, H. Košice, IMR SAS 2005, p. 200.
[30] MITCHELL, S. C.—BAUMGAERTNER, F.: In: Deformation and Fracture in Structural PM Materials, DFPM 2005. Eds.: Parilák, Ľ., Danninger, H. Košice, IMR SAS 2005, p. 11.